Effects of sulfur on dehydrogenation of methylcyclohexane over platinum catalysts

Supplementary Information

Felicia Zaar,* Alvaro Posada-Borbón, and Henrik Grönbeck*

Department of Physics and Competence Centre of Catalysis, Chalmers University of Technology, Gothenburg, Sweden

E-mail: felicia.zaar@chalmers.se; ghj@chalmers.se

Convergence tests

Convergence tests were conducted to determine the plane-wave cutoff energy E_{cut}, the size of the k-point grid (N x N x M), the first order Methfessel-Paxton smearing width σ, and the theoretical lattice constant a_0. The smearing width and the lattice constant were evaluated by calculating the cohesive energy E_{coh} of face centered cubic (fcc) bulk Pt, using a (12 x 12 x 12) k-point grid and a plane-wave cutoff of 450 eV. Noting that the cohesive energy varied only marginally with the smearing width, σ was fixed at 0.1 eV for all subsequent calculations. The lattice constant was set to the experimental value, 3.92 , which was accurately reproduced through the inclusion of dispersion corrections.

Convergence of the k-point grid and the plane-wave cutoff was assessed using the adsorption energy of CO in a top-site configuration on a p(4 x 4) Pt(111) slab with five atomic layers. The k-point grid was varied from (2 x 2 x 1) to (10 x 10 x 1) using a plane-wave cutoff of 480 eV, whereas the plane-wave cutoff was varied from 300 to 550 eV using a (6 x 6 x 1) k-point grid. With a (6 x 6 x 1) grid and a 450 eV cutoff, the adsorption energy is converged within 0.002 eV relative the largest grid and the highest cutoff tested. However, considering the extent of the computational study, a (4 x 4 x 1) grid was adopted to limit computational cost; at this sampling, the adsorption energy of CO is converged within 0.037 eV. No definitive trend in the CO adsorption energy was observed with respect to slab thickness, but the change in charge density induced by sulfur was noted to reach into the fourth atomic layer of Pt(111). Therefore, a five-layer slab was chosen as a reasonable compromise between accuracy and computational cost. The convergence results are summarized Fig. S1.

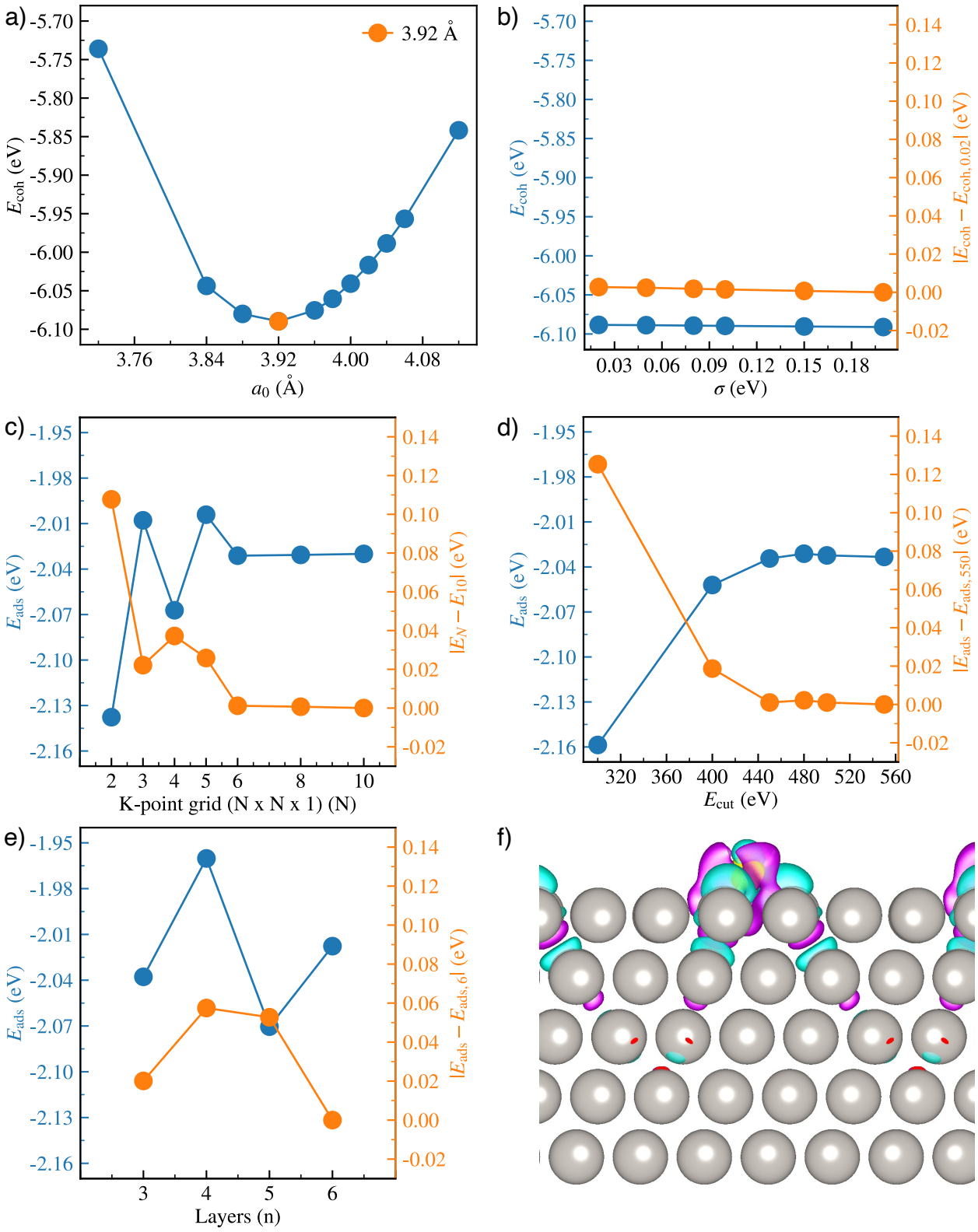

Fig. S1 Convergence study of a) the theoretical lattice constant a_0, b) the smearing width σ, c) the k-point grid (N x N x 1), d) the plane-wave cutoff energy E_{cut} and e) the number of layers in the slab n. f) The charge density difference induced by sulfur in Pt(111). Settings: a-b) $E_{\mathrm{cut}} = 450\,\mathrm{eV}$, (12 x 12 x 12); c) $E_{\mathrm{cut}} = 480\,\mathrm{eV}$; d) (6 x 6 x 1); e-f) $E_{\mathrm{cut}} = 450\,\mathrm{eV}$, (4 x 4 x 1); a, c-f) $\sigma = 0.1\,\mathrm{eV}$

Electronic and structural effects of sulfur on Pt and CO

Surface strain

The surface strain is defined as the distance between neighboring Pt atoms relative the interatomic distance in Pt-bulk ($\Delta d/d_0 = (d - d_0)/d_0$ where $d_0 = 2.772\,\text{Å}$) and is expected to correlate linearly with adsorption energy.[1] Fig. S2 shows the adsorption energy of sulfur in fcc configuration on Pt(111) as function of surface strain, which was introduced into the slab by varying the lattice constant a between $0.98a_0$ and $1.02a_0$.

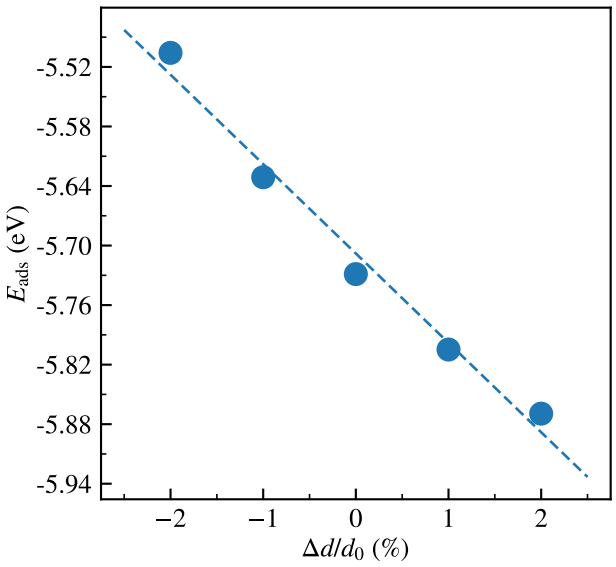

Fig. S2 Adsorption energy of sulfur in an fcc site on Pt(111), as a function of surface strain, including a linear fit.

d-band centers

Projected, atomic d-band centers (ε_d) where calculated for pristine and sulfur-modified Pt(111) and Pt(553), as the first moment of the projected d-band density of states ρ_d relative the Fermi level (ε_F):

$$\varepsilon_\text{d} = \frac{\int_{-\infty}^{\varepsilon_\text{F}} \varepsilon \rho_\text{d}(\varepsilon) d\varepsilon}{\int_{-\infty}^{\varepsilon_\text{F}} \rho_\text{d}(\varepsilon) d\varepsilon} \tag{1}$$

Shifts in the d-band centers induced by adsorption of sulfur were then calculated as:

$$\Delta\varepsilon_{\mathrm{d}} = \varepsilon_{\mathrm{d}}(\mathrm{S/slab}) - \varepsilon_{\mathrm{d}}(\mathrm{slab}) \tag{2}$$

As shown in Fig. S3, adsorption of sulfur results in a local downward shift of the atomic d-band centers on both Pt(111) and Pt(553). This effect is most pronounced for Pt atoms directly bound to sulfur, although a modest downward shift is also observed across the entire top layer of Pt(111). On Pt(553), by contrast, the influence of sulfur on Pt atoms beyond its immediate neighbors is negligible, and the overall downward shift is smaller. These differences in behavior between the two surfaces likely arise from variations in both Pt coordination at the sulfur adsorption sites and surface strain. Specifically, the higher intrinsic strain of Pt(553) relative to Pt(111), together with the lower coordination number of sulfur-bonded Pt atoms at the Pt(553) step edge compared to the fcc sites on Pt(111), would partially counteract the sulfur-induced downward shift of the d-band centers on Pt(553).

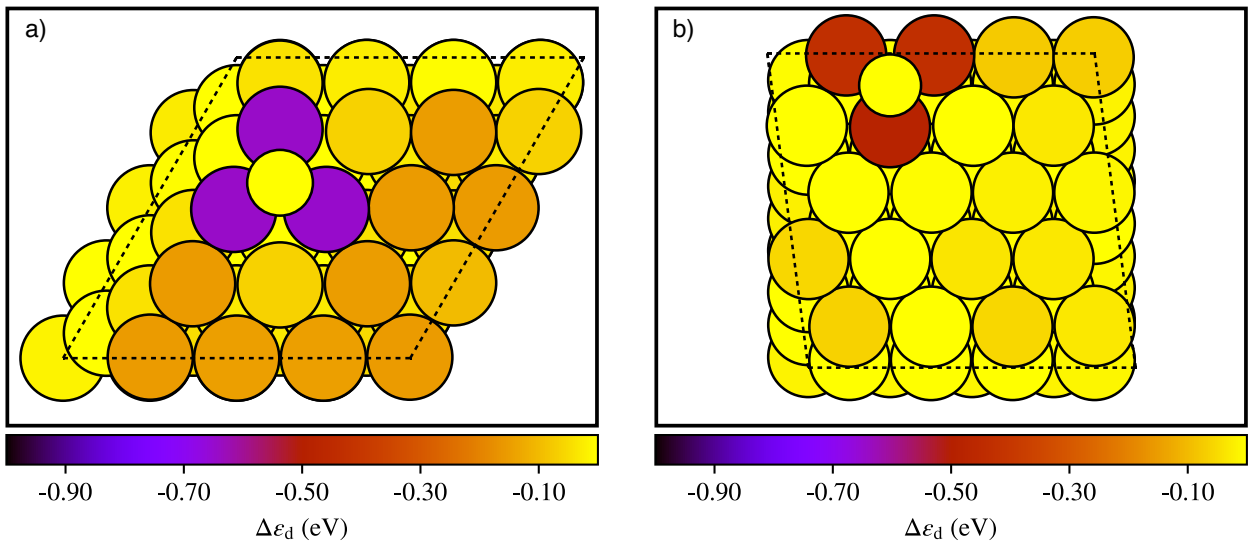

Fig. S3 d-band center shifts induced by sulfur adsorption relative the pristine surface on a) Pt(111) and b) Pt(553). The illustrations were made using the Atomic Simulation Environment (ASE).[2]

Vibrational modes

Vibrational modes were calculated for CO in bridge configuration on sulfur-modified Pt(100), Pt(111), Pt(223) and Pt(553), applying two different S-CO distances: < 3.4 Å and > 4.9 Å). The vibrational modes were obtained using the harmonic approximation, using two-point finite differences with 0.015 steps. On all surfaces, the wavenumber of the CO stretching mode shifted to higher values with decreasing distance to sulfur (see Fig. S4), in agreement with experimental observations by Auer et al.[3]

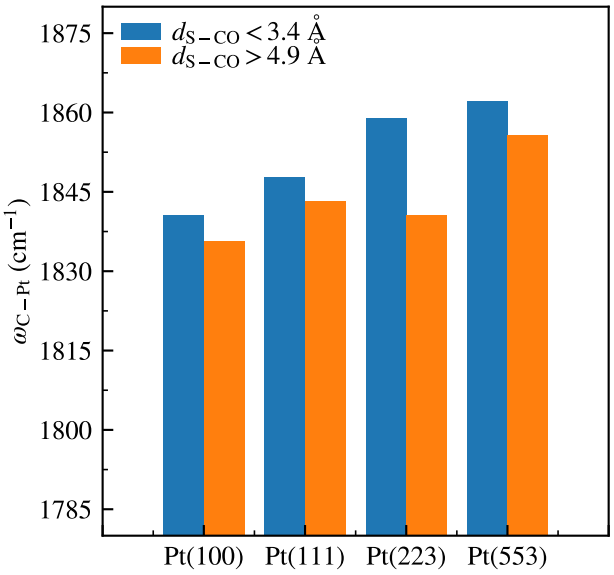

Fig. S4 Wavenumbers of the CO stretching vibrational mode at different S-CO distances on Pt(100), Pt(111), Pt(223) and Pt(553).

Adsorption properties

Adsorption of sulfur and CO

Considered adsorption sites and adsorption energies of sulfur and CO are collected in Tables S1 and S2, respectively (a schematic illustration of considered sites is given in Fig. 2 of the main text). Fig. S5 shows adsorption energies and configurations of sulfur at 50%, 75% and 100% coverage of the step edge of Pt(553), and for reference, the adsorption of sulfur on the

Pt(553) terrace. From this analysis, it is clear that adsorption on the terrace is preferable over step edge coverage above 50%.

Table S1 Adsorption sites and adsorption energies of sulfur with respect to gas phase atomic sulfur on Pt(100), Pt(111), Pt(223) and Pt(553). "–" indicates a structure that relaxed into one already obtained.

Surface	Initial adsorption site	Final Adsorption site	E_{ads} (eV)
Pt(100)	hollow	hollow	-6.164
	bridge	bridge	-5.304
	top	top	-3.757
Pt(111)	fcc hollow	fcc hollow	-5.729
	hcp hollow	hcp hollow	-5.533
	top	top	-3.567
	bridge	fcc hollow	–
Pt(223)	step edge hcp hollow	step edge hcp hollow	−5.667
	terrace fcc hollow	terrace fcc hollow	−5.589
	step hcp hollow	step hcp hollow	−5.489
	step edge top	step edge fcc hollow	−5.531
	terrace hcp hollow	terrace hcp hollow	−5.339
	step bottom hcp hollow	step bottom hcp hollow	−5.275
	step bottom bridge	step bottom hcp hollow	–
	step bottom fcc hollow	step bottom fcc hollow	–
	step bridge[a]	step hcp hollow	–
	step edge bridge	step edge fcc hollow	–
	step edge fcc hollow	step edge fcc hollow	–
	terrace top	terrace hcp hollow	–
	terrace bridge	terrace hcp hollow	–
Pt(553)	step edge fcc hollow	step edge fcc hollow	−5.562
	terrace fcc hollow	terrace fcc hollow	−5.447
	terrace hcp hollow	terrace hcp hollow	−5.319
	step edge hcp hollow	step edge hcp hollow	−5.303
	step fcc hollow[a]	step fcc hollow	−5.178
	step edge bridge	step edge bridge	−5.04
	step hcp hollow	step hcp hollow	−4.751
	step bottom bridge	step fcc hollow	–
	step bottom fcc hollow	step bottom fcc hollow	–
	step bottom top	terrace fcc hollow	–
	step bridge	step fcc hollow	–
	step edge top	step edge bridge	–
	terrace bridge	terrace fcc hollow	–
	terrace top	terrace fcc hollow	–

[a] Same as step bottom top.

Table S2 Adsorption sites and adsorption energies of CO with respect to gas phase CO on Pt(100), Pt(111), Pt(223) and Pt(553). "–" indicates a structure that relaxed into one already obtained.

Surface	Initial adsorption site	Final Adsorption site	E_{ads} (eV)
Pt(100)	bridge	bridge	−2.494
	top	top	−2.286
	hollow	top	–
Pt(111)	fcc hollow	fcc hollow	−2.158
	bridge	bridge	−2.130
	hcp hollow	hcp hollow	−2.124
	top	top	−2.070
Pt(223)	step edge bridge	step edge bridge	−2.438
	step edge top	step edge top	−2.323
	step bridge	step bridge	−2.165
	step bottom top	step bottom top	−2.165
	terrace fcc hollow	terrace fcc hollow	−2.131
	terrace bridge	terrace bridge	−2.086
	terrace hcp hollow	terrace hcp hollow	−2.044
	step bottom hcp hollow	step bottom hcp hollow	−2.041
	step bottom bridge	step bottom bridge	−1.987
	step edge fcc hollow	step edge fcc hollow	−1.986
	step bottom fcc hollow	step bottom fcc hollow	−1.925
	terrace top	terrace top	−1.886
	step edge hcp hollow	step edge bridge	–
	step hcp hollow	step edge bridge	–
Pt(553)	step edge top	step edge top	−2.260
	step edge bridge	step edge bridge	−2.171
	terrace bridge	terrace bridge	−2.094
	step bottom hcp hollow	step bottom hcp hollow	−2.091
	terrace hcp hollow	terrace hcp hollow	−2.091
	terrace fcc hollow	terrace fcc hollow	−2.088
	step edge fcc hollow	step edge fcc hollow	−2.059
	step bottom top	step bottom top	−1.949
	terrace top	terrace top	−1.829
	step bottom bridge	step bottom top	–
	step bottom fcc hollow	terrace bridge	–
	step bridge	step edge bridge	–
	step edge hcp hollow	step edge top	–
	step fcc hollow	step edge bridge	–
	step hcp hollow	step edge bridge	–

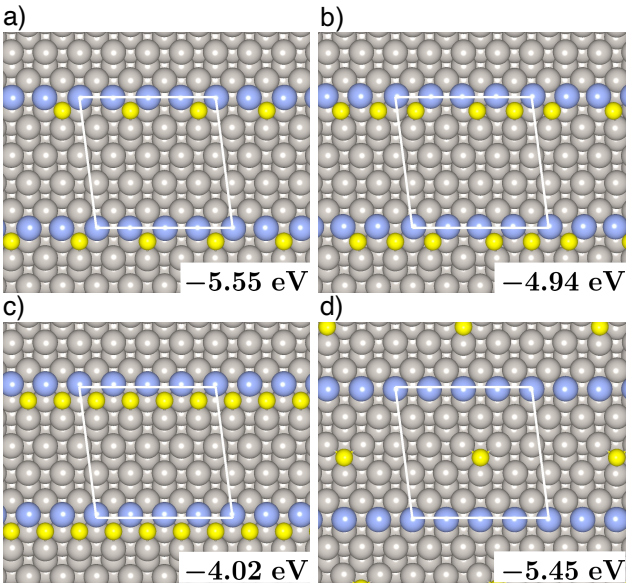

Fig. S5 Adsorption configurations and energies of sulfur on Pt(553) at a) 50%, b) 75% and c) 100% coverage of the step edge. d) Adsorption of sulfur on the Pt(553) terrace.

Adsorption of C_7H_8 and C_7H_{14}

The considered sites and orientations of C_7H_8 and C_7H_{14}, in addition to the sites discussed in the main text, are schematically illustrated in Fig. S6. All adsorption configurations, except for the configurations at the step, initially have two C-C bonds of the C-H ring aligned along the x or the y-axis (the z-axis coincides with the surface normal). At the step, two C-C bonds will instead be aligned in either the yz plane or the xz plane. Accordingly, adsorption configurations of C_7H_8 and C_7H_{14} are denoted by, for example, "fcc hollow x" or "step fcc hollow yz". For some configurations, structural relaxation results in an intermediate rotation of the molecule. In these cases, the final adsorption site is denoted by, e.g., "fcc hollow xy" or "step fcc hollow xyz". All configuration are also distinguished by the carbon atom to which the methyl group is bound, i.e. C1, C2, C3 or C4, where C1 is always the carbon atom with the highest y-coordinate.

For each rotation of the molecule, there are multiple possible bridge configurations on Pt(553). On the terrace of this surface, the molecule may adsorb with C1 and C4, or with C2 and C5, directly above Pt atoms. These configurations are indicated by "aligned" and

"diagonal" bridge, respectively, to reflect whether or not the bridge is aligned along the x-axis. At the step edge, a bridge configuration may involve two or four C-Pt bonds, marked as "small" or "large" bridge. Finally, for C_7H_{14} we distinguish between the initial directions of the C-H bond at the ipso-carbon by "down" or "up", depending on if the H atom is directed toward or away from the surface. Knowing that benzene is unstable in top sites,[4] these sites were excluded from the study. All adsorption sites and energies calculated for C_7H_8 and C_7H_{14} are collected in Table S3 and S4, respectively.

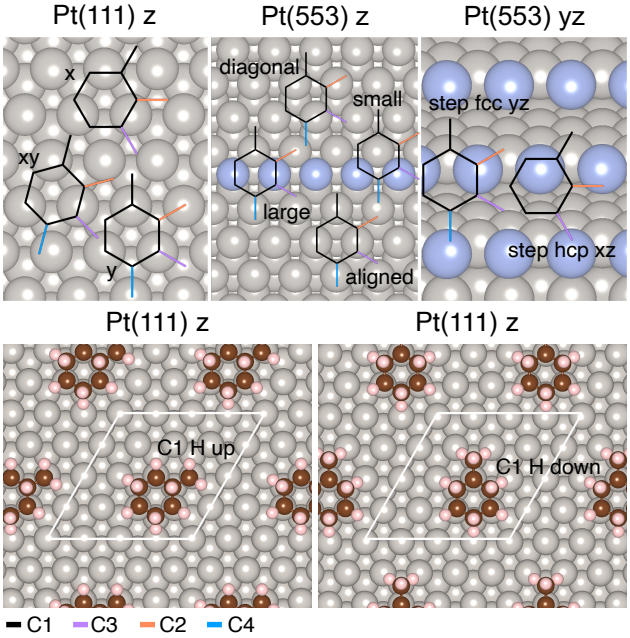

Fig. S6 Additional configurational space for adsorbed C_7H_8 and C_7H_{14}, both represented by the molecular structures in the upper panel. Black, orange, purple and blue branches indicate different placements of the methyl group, denoted by C1, C2, C3 and C4, respectively. The upper middle panel shows the configurations here denoted by aligned, diagonal, small and large bridge. To the upper right, step fcc and step hcp sites are displayed. In the lower panel, the two different investigated z-rotations of C_7H_{14} are shown (H at the ipso-carbon toward or away from the surface). "z" and "yz" in the headings indicate the axis or plane along which the image is oriented.

Table S3 Adsorption sites and energies of C_7H_8 Pt(111) and Pt(553). "–" indicates a structure that relaxed into one already obtained.

Surface	Initial adsorption site	Final Adsorption site	E_{ads} (eV)
Pt(111)	diagonal bridge C1 y	diagonal bridge C1 y	−2.784
	aligned bridge C2 y	aligned bridge C2 y	−2.719
	fcc hollow C2 y	diagonal bridge C2 y	−2.718

Pt(111)	fcc hollow C1 x	fcc hollow C1 x	−2.387
	fcc hollow C2 x	fcc hollow C2 x	−2.387
	aligned bridge C1 x	aligned bridge C1 x	−2.181
	aligned bridge C2 x	aligned bridge C2 x	−2.110
	aligned bridge C1 y	diagonal bridge C1 y	–
	fcc hollow C1 y	diagonal bridge C1 y	–
	hcp hollow C1 y	diagonal bridge C1 y	–
Pt(553)	step fcc hollow C2 xz	step fcc hollow C2 xz	−3.065
	step fcc hollow C3 xz	step fcc hollow C3 xz	−3.053
	step fcc hollow C1 xz	edge small aligned bridge C1 x	−2.732
	edge large aligned bridge C3 x	edge small aligned bridge C3 x	−2.705
	edge large aligned bridge C2 x	edge small aligned bridge C2 x	−2.702
	edge large aligned bridge C1 x	edge large aligned bridge C1 x	−2.6
	edge large aligned bridge C1 y	edge large aligned bridge C1 y	−2.598
	edge fcc hollow C1 x	edge fcc hollow C1 x	−2.584
	edge fcc hollow C3 x	edge fcc hollow C3 x	−2.558
	edge fcc hollow C2 x	edge fcc hollow C2 x	−2.511
	edge hcp hollow C1 y	edge diagonal bridge C1 y	−2.502
	edge hcp hollow C4 y	edge diagonal bridge C4 y	−2.487
	step bottom fcc hollow C1 y	step fcc hollow C1 xyz	−2.452
	edge large aligned bridge C2 y	edge large aligned bridge C2 y	−2.425
	edge fcc hollow C2 y	edge fcc hollow C2 y	−2.423
	edge large aligned bridge C3 y	edge large aligned bridge C3 y	−2.408
	terrace aligned bridge C3 y	terrace aligned bridge C3 y	−2.401
	terrace aligned bridge C4 y	terrace aligned bridge C4 y	−2.391
	terrace aligned bridge C2 y	terrace aligned bridge C2 y	−2.374
	edge fcc hollow C4 y	edge large aligned bridge C4 y	−2.373
	terrace aligned bridge C1 y	terrace aligned bridge C1 y	−2.341
	upper terrace aligned bridge C3 y	upper terrace aligned bridge C3 y	−2.285
	upper terrace aligned bridge C4 y	upper terrace aligned bridge C4 y	−2.282
	upper terrace aligned bridge C2 y	upper terrace aligned bridge C2 y	−2.257
	upper terrace aligned bridge C1 y	upper terrace aligned bridge C1 y	−2.208
	upper terrace hcp hollow C4 y	upper terrace diagonal bridge C4 y	−2.192
	terrace hcp hollow C4 y	terrace diagonal bridge C4 y	−2.191
	step bottom hcp hollow C3 y	step diagonal bridge C3 xyz	−2.18
	step bottom fcc hollow C3 x	step bottom fcc hollow C3 x	−2.161
	upper terrace fcc hollow C1 y	upper terrace diagonal bridge C1 y	−2.14
	edge hcp hollow C3 x	edge hcp hollow C3 x	−2.138
	upper terrace hcp hollow C1 x	upper terrace hcp hollow C1 x	−2.112
	edge hcp hollow C1 x	edge hcp hollow C1 x	−2.112
	upper terrace hcp hollow C2 x	upper terrace hcp hollow C2 x	−2.094
	edge hcp hollow C2 x	edge hcp hollow C2 x	−2.094
	terrace aligned bridge C3 x	terrace aligned bridge C3 x	−2.087
	terrace aligned bridge C1 x	terrace fcc hollow C1 x	−2.041
	terrace fcc hollow C2 x	terrace fcc hollow C2 x	−1.993
	terrace aligned bridge C2 x	terrace aligned bridge C2 x	−1.966
	upper terrace aligned bridge C3 x	upper terrace aligned bridge C3 x	−1.963
	terrace fcc hollow C1 x	terrace fcc hollow C1 x	−1.962

	step bottom aligned bridge C1 x	step bottom aligned bridge C1 x	−1.929
	upper terrace fcc hollow C3 x	upper terrace fcc hollow C3 x	−1.907
	terrace fcc hollow C3 x	terrace fcc hollow C3 x	−1.897
	step bottom hcp hollow C3 x	step bottom hcp hollow C3 x	−1.89
	upper terrace hcp hollow C3 x	upper terrace hcp hollow C3 x	−1.888
	terrace hcp hollow C3 x	terrace hcp hollow C3 x	−1.888
	step bottom hcp hollow C2 x	step bottom hcp hollow C2 x	−1.862
	upper terrace fcc hollow C1 x	upper terrace fcc hollow C1 x	−1.861
	upper terrace fcc hollow C2 x	upper terrace fcc hollow C2 x	−1.861
	terrace hcp hollow C1 x	terrace hcp hollow C1 x	−1.837
	step bottom hcp hollow C1 y	step bottom hcp hollow C1 y	−1.834
	step bottom aligned bridge C1 y	step bottom aligned bridge C1 y	−1.834
	upper terrace aligned bridge C2 x	upper terrace aligned bridge C2 x	−1.772
	bystep hcp hollow C3 x	bystep hcp hollow C3 x	−1.749
	step bottom hcp hollow C4 y	step bottom aligned bridge C4 y	−1.742
	edge fcc hollow C1 y	edge large aligned bridge C1 y	–
	edge fcc hollow C3 y	edge fcc hollow C3 x	–
	edge hcp hollow C2 y	upper terrace aligned bridge C2 y	–
	edge hcp hollow C3 y	upper terrace aligned bridge C3 y	–
	edge top C1 y	edge diagonal bridge C1 y	–
	edge top C2 x	edge diagonal bridge C3 y	–
	step bottom aligned bridge C2 x	step fcc hollow C2 xz	–
	step bottom aligned bridge C2 y	step fcc hollow C2 xz	–
	step bottom aligned bridge C3 x	step fcc hollow C3 xz	–
Pt(553)	step bottom aligned bridge C3 y	step fcc hollow C2 xz	–
	step bottom aligned bridge C4 y	step fcc hollow C3 xz	–
	step bottom fcc hollow C1 x	edge small aligned bridge C1 x	–
	step bottom fcc hollow C2 x	step fcc hollow C2 xz	–
	step bottom fcc hollow C2 y	step fcc hollow C2 xz	–
	step bottom fcc hollow C3 y	step fcc hollow C2 xz	–
	step bottom fcc hollow C4 y	step fcc hollow C3 xz	–
	step bottom hcp hollow C1 x	edge small aligned bridge C1 x	–
	step bottom hcp hollow C2 y	step fcc hollow C2 xz	–
	step fcc hollow C1 yz	edge small aligned bridge C1 x	–
	step fcc hollow C2 yz	edge small aligned bridge C1 x	–
	step fcc hollow C3 yz	step fcc hollow C2 xz	–
	step fcc hollow C4 yz	step fcc hollow C3 xz	–
	step hcp hollow C1 x	edge small aligned bridge C1 x	–
	step hcp hollow C2 x	edge small aligned bridge C1 x	–
	step hcp hollow C2 yz	edge small aligned bridge C1 x	–
	step hcp hollow C1 yz	edge small aligned bridge C1 x	–
	step hcp hollow C4 yz	edge small aligned bridge C3 x	–
	step hcp hollow C3 xz	edge small aligned bridge C3 x	–
	step hcp hollow C3 yz	edge small aligned bridge C2 x	–
	terrace fcc hollow C1 y	terrace aligned bridge C1 y	–
	terrace fcc hollow C2 y	terrace aligned bridge C2 y	–
	terrace fcc hollow C3 y	terrace aligned bridge C3 y	–
	terrace fcc hollow C4 y	terrace aligned bridge C4 y	–

	terrace hcp hollow C1 y	terrace aligned bridge C1 y	–
	terrace hcp hollow C2 x	terrace aligned bridge C2 x	–
	terrace hcp hollow C2 y	terrace aligned bridge C2 y	–
	terrace hcp hollow C3 y	terrace aligned bridge C3 y	–
	terrace hcp hollow C4 y	terrace aligned bridge C4 y	–
Pt(553)	upper terrace aligned bridge C1 x	upper terrace aligned bridge C1 y	–
	upper terrace hcp hollow C1 y	upper terrace aligned bridge C1 y	–
	upper terrace hcp hollow C2 y	upper terrace aligned bridge C2 y	–
	upper terrace hcp hollow C3 y	upper terrace aligned bridge C3 y	–
	upper terrace fcc hollow C2 y	upper terrace aligned bridge C2 y	–
	upper terrace fcc hollow C3 y	upper terrace aligned bridge C3 y	–
	upper terrace fcc hollow C4 y	upper terrace aligned bridge C4 y	–

Table S4 Adsorption sites and adsorption energies of C_7H_{14} Pt(111) and Pt(553). "–" indicates a structure that relaxed into one already obtained.

Surface	Initial adsorption site	Final Adsorption site	E_{ads} (eV)
	fcc hollow C3 y H down	fcc hollow C3 y	−1.493
	fcc hollow C1 x H down	fcc hollow C1 y	−1.491
	fcc hollow C2 y H down	hcp hollow C2 y	−1.490
	fcc hollow C2 y	fcc hollow C2 y	−1.445
	hcp hollow C1 y	hcp hollow C1 y	−1.443
Pt(111)	fcc hollow C3 y	hcp hollow C3 y	−1.442
	aligned bridge C1 y	aligned bridge C1 y	−1.439
	diagonal bridge C1 y	hcp hollow C1 y	−1.434
	fcc hollow C1 y	fcc hollow C1 y	−1.163
	aligned bridge C1 y H down	fcc hollow C1 x	–
	fcc hollow C1 x	fcc hollow C2 y	–
	hcp hollow C1 y H down	fcc hollow C1 y	–
	step bottom hcp C2 x	step bottom hcp C3 xy	−1.568
	step bottom hcp C3 x	step bottom hcp C4 xy	−1.544
	step bottom aligned bridge C2 x	step bottom fcc C2 xy	−1.533
	step bottom fcc C2 x	step bottom fcc C2 x	−1.518
	terrace fcc C3 y	step bottom top C3 y	−1.513
	step fcc hollow C2 xz	step fcc hollow C2 xz	−1.512
	step fcc hollow C3 yz	step fcc hollow C3 xyz	−1.505
	step bottom fcc hollow C1 x	step bottom fcc hollow C1 xy	−1.496
	step fcc hollow C1 xz	step fcc hollow C1 xyz	−1.493
Pt(553)	step bottom hcp hollow C1 y	step bottom hcp hollow C1 y	−1.482
	step bottom hcp hollow C1 x	step bottom hcp hollow C1 xy	−1.481
	edge small aligned bridge C3 x	step fcc hollow C3 xyz	−1.480
	terrace fcc hollow C1 y	terrace hcp hollow C1 xy	−1.480
	step fcc hollow C3 xz	step fcc hollow C3 xyz	−1.479
	step bottom fcc hollow C1 y	step fcc hollow C1 yz	−1.476
	step hcp hollow C3 xz	step diagonal bridge C3 xyz	−1.476
	edge small aligned bridge C3 y	step fcc hollow C3 xyz	−1.474
	step fcc hollow C1 yz	step fcc hollow C1 yz	−1.473

Pt(553)	step fcc hollow C2 yz	edge small aligned bridge C2 y	−1.471
	edge small aligned bridge C1 y	step fcc hollow C1 yz	−1.469
	edge large aligned bridge C1 x	edge large aligned bridge C1 x	−1.466
	edge small aligned bridge C1 x	edge small aligned bridge C2 xy	−1.461
	step hcp hollow C1 xz	step diagonal bridge C1 xy	−1.459
	step hcp hollow C2 yz	step hcp hollow C2 yz	−1.458
	step bottom aligned bridge C3 x	step bottom fcc hollow C3 xy	−1.435
	terrace aligned bridge C4 y	terrace fcc hollow C4 xy	−1.432
	terrace fcc hollow C3 x	terrace fcc hollow C3 xy	−1.431
	terrace fcc hollow C4 y	terrace fcc hollow C4 y	−1.431
	step fcc hollow C4 yz	step diagonal bridge C3 xyz	−1.427
	edge fcc hollow C1 x	edge large aligned bridge C2 y	−1.425
	terrace fcc hollow C2 y	terrace fcc hollow C2 y	−1.423
	terrace fcc hollow C2 x	terrace fcc hollow C2 x	−1.422
	edge fcc hollow C2 x	edge fcc hollow C2 x	−1.421
	edge hcp hollow C2 y	edge large aligned bridge C2 y	−1.420
	edge fcc hollow C4 y	edge fcc hollow C4 y	−1.420
	step hcp hollow C4 yz	step hcp hollow C4 yz	−1.417
	edge fcc hollow C2 y	edge large aligned bridge C2 x	−1.414
	edge hcp hollow C4 y	edge fcc hollow C4 y	−1.414
	edge fcc hollow C3 x	edge fcc hollow C3 x	−1.409
	edge fcc hollow C3 y	edge hcp hollow C3 y	−1.387
	step bottom hcp hollow C3 y	step bottom hcp hollow C3 y	−1.386
	edge hcp hollow C3 x	edge hcp hollow C3 x	−1.386
	edge hcp hollow C3 y	edge hcp hollow C3 y	−1.386
	edge large aligned bridge C4 y	edge large aligned bridge C4 y	−1.379
	edge large aligned bridge C3 x	edge large aligned bridge C3 xy	−1.378
	edge small aligned bridge C4 y	edge small aligned bridge C4 y	−1.357
	upper terrace fcc hollow C4 y	upper terrace fcc hollow C4 y	−1.338
	edge small aligned bridge C2 y	edge small aligned bridge C2 y	−1.338
	upper terrace fcc hollow C3 x	upper terrace fcc hollow C3 x	−1.338
	upper terrace aligned bridge C4 y	upper terrace aligned bridge C4 y	−1.337
	terrace hcp hollow C4 y	terrace fcc hollow C4 y	−1.332
	terrace hcp hollow C3 y	terrace hcp hollow C3 y	−1.327
	edge hcp hollow C1 y	edge hcp hollow C1 y	−1.322
	edge hcp hollow C1 x	edge hcp hollow C1 x	−1.319
	edge large aligned bridge C2 y	edge large aligned bridge C2 y	−1.315
	edge large aligned bridge C2 x	edge large aligned bridge C2 xy	−1.307
	step bottom hcp hollow C4 y	step fcc hollow C4 yz	−1.304
	step bottom aligned bridge C4 y	step bottom aligned bridge C4 y	−1.302
	upper terrace fcc hollow C3 y	edge hcp hollow C3 y	−1.287
	upper terrace hcp hollow C3 y	upper terrace hcp hollow C3 y	−1.286
	upper terrace aligned bridge C3 y	upper terrace aligned bridge C3 y	−1.284
	terrace hcp hollow C1 y	terrace hcp hollow C1 y	−1.279
	upper terrace fcc hollow C1 y	upper terrace hcp hollow C1 y	−1.277
	terrace aligned bridge C1 y	terrace aligned bridge C1 y	−1.277
	upper terrace aligned bridge C2 y	upper terrace aligned bridge C2 y	−1.273
	upper terrace fcc hollow C2 y	upper terrace fcc hollow C2 y	−1.273

	upper terrace fcc hollow C2 x	upper terrace fcc hollow C2 x	−1.271
	step bottom top C4 y	step bottom hcp hollow C4 y	−1.271
	upper terrace fcc hollow C1 x	upper terrace fcc hollow C2 xy	−1.263
	terrace aligned bridge C3 x	terrace aligned bridge C3 x	−1.262
	upper terrace aligned bridge C1 y	upper terrace hcp hollow C1 y	−1.248
	upper terrace hcp hollow C1 x	upper terrace hcp hollow C1 x	−1.216
	edge top C1 y	edge top C1 y	−1.214
	upper terrace hcp hollow C1 yz	upper terrace hcp hollow C1 y	−1.214
	upper terrace aligned bridge C3 x	upper terrace aligned bridge C3 x	−1.135
	edge top C2 x	edge top C2 xy	−1.117
	edge fcc hollow C1 y	edge hcp hollow C1 y	–
	edge hcp hollow C2 x	edge hcp hollow C3 y	–
	edge large aligned bridge C1 y	step fcc hollow C1 xyz	–
	edge large aligned bridge C3 y	edge small aligned bridge C2 xy	–
	edge small aligned bridge C2 x	edge small aligned bridge C2 y	–
	step bottom aligned bridge C1 x	step bottom fcc hollow C1 xy	–
	step bottom aligned bridge C1 y	step bottom hcp hollow C1 y	–
	step bottom aligned bridge C2 y	step bottom fcc hollow C2 xy	–
Pt(553)	step bottom aligned bridge C3 y	step bottom hcp hollow C3 xy	–
	step bottom fcc hollow C2 y	step bottom fcc hollow C2 xy	–
	step bottom hcp hollow C2 y	terrace fcc hollow C2 y	–
	step bottom top C2 x	step bottom hcp hollow C3 xy	–
	step hcp hollow C1 yz	step fcc hollow C1 xyz	–
	step hcp hollow C2 xz	step bottom hcp hollow C3 xy	–
	step hcp hollow C3 yz	edge small aligned bridge C2 xy	–
	terrace aligned bridge C1 x	terrace fcc hollow C2 y	–
	terrace aligned bridge C2 x	terrace hcp hollow C3 y	–
	terrace aligned bridge C2 y	terrace fcc hollow C2 y	–
	terrace aligned bridge C3 y	terrace hcp hollow C3 y	–
	terrace fcc hollow C1 x	terrace fcc hollow C2 y	–
	terrace hcp hollow C1 x	terrace fcc hollow C2 y	–
	terrace hcp hollow C2 x	terrace fcc hollow C2 y	–
	terrace hcp hollow C2 y	terrace fcc hollow C2 y	–
	terrace hcp hollow C3 x	terrace hcp hollow C3 y	–
	upper terrace aligned bridge C1 x	upper terrace fcc hollow C2 y	–
	upper terrace aligned bridge C2 x	upper terrace fcc hollow C2 y	–
	upper terrace hcp hollow C2 x	upper terrace hcp hollow C3 y	–
	upper terrace hcp hollow C2 y	upper terrace fcc hollow C2 y	–

Dehydrogenation of C_7H_{14}

Energetics of intermediates

The dehydrogenation reaction was modeled by stepwise removal of H from C_7H_{14} on Pt(111) modified with a 3/16 monolayer (ML) of sulfur. Fig. S7 illustrates the ${C_7H_{14}}^* \longrightarrow$

$C_7H_{13}^* + H^*$ step as a representative example. First, the structure of C_7H_{13} was identified by removing H from all symmetry-inequivalent sites. Thereafter, the $C_7H_{13}^* + H^*$ configuration was determined by placing H at various adsorption sites in the immediate vicinity of the dehydrogenated carbon. Structures without sulfur were obtained by removing sulfur from the corresponding sulfur-modified structures, followed by structural relaxation. This procedure was repeated for all remaining reaction steps, generating the reaction energetics summarized in Table S5 (spin polarization settings of intermediates and atoms are shown in Table S6). It should be noted that reaction energies may be slightly overestimated, in particular on the pristine surface, as a full configurational search not was done in the absence of sulfur. For example, removing the CH_3 group from $C_7H_8^*$ yields $C_6H_5^*$ adsorbed in a diagonal bridge C1 configuration, corresponding to a reaction energy of 1.28 eV. However, this adsorption geometry is marginally less stable than the aligned bridge C1 configuration, which could potentially be accessed via diffusion and would result in a reaction energy of 1.21 eV.

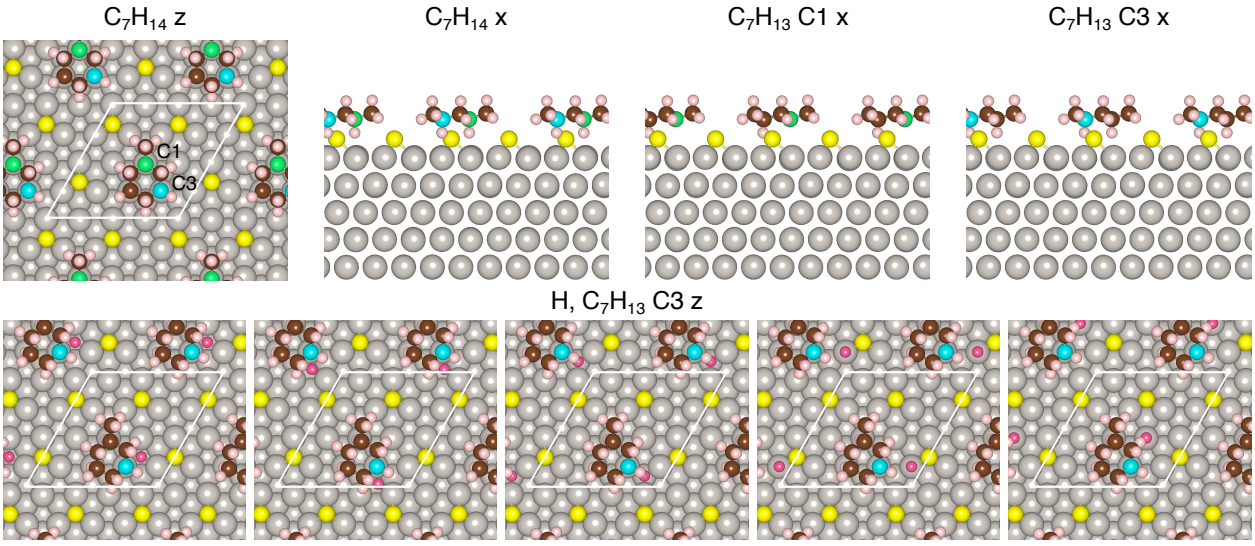

Fig. S7 $C_7H_{14}^* \longrightarrow C_7H_{13}^* + H^*$ over Pt(111) modified with 3/16 ML sulfur. The upper panel shows C_7H_{14} and two versions of C_7H_{13}, where H has been removed from site C1 (green) and C3 (blue), respectively. The lower panel shows initial placements of H (pink) in the vicinity of the C3 version of C_7H_{13}, which was found to be most stable. "z" and "x" in the headings indicate the axis along which the image is oriented.

Table S5 Relative and reaction energies during dehydrogenation of C_7H_{14}. The surface is denoted by $*$.

	Reaction	[a]E_{rel} (eV)	[b]E_{rel} (eV)	[c]ΔE_r (eV)	[d]ΔE_r (eV)
dehyd.	$C_7H_{14}(g) + * \longrightarrow C_7H_{14}^*$	−1.491	−1.462	−1.491	−1.462
	$C_7H_{14}^* \longrightarrow C_7H_{13}^* + H^*$	−1.477	−1.379	0.014	0.083
	$C_7H_{13}^* + H^* \longrightarrow C_7H_{13}^* + 1/2H_2(g)$	−1.108	−1.055	0.369	0.324
	$C_7H_{13}^* \longrightarrow C_7H_{12}^* + H^*$	−1.240	−1.090	−0.132	−0.035
	$C_7H_{12}^* + H^* \longrightarrow C_7H_{12}^* + 1/2H_2(g)$	−0.769	−0.702	0.472	0.388
	$C_7H_{12}^* \longrightarrow C_7H_{11}^* + H^*$	−0.998	−0.741	−0.230	−0.039
	$C_7H_{11}^* + H^* \longrightarrow C_7H_{11}^* + 1/2H_2(g)$	−0.648	−0.458	0.350	0.283
	$C_7H_{11}^* \longrightarrow C_7H_{10}^* + H^*$	−0.757	−0.376	−0.109	0.082
	$C_7H_{10}^* + H^* \longrightarrow C_7H_{10}^* + 1/2H_2(g)$	−0.386	−0.122	0.371	0.254
	$C_7H_{10}^* \longrightarrow C_7H_9^* + H^*$	−0.635	0.154	−0.249	0.276
	$C_7H_9^* + H^* \longrightarrow C_7H_9^* + 1/2H_2(g)$	−0.103	0.365	0.533	0.216
	$C_7H_9^* \longrightarrow C_7H_8^* + H^*$	−0.351	0.379	−0.248	0.014
	$C_7H_8^* + H^* \longrightarrow C_7H_8^* + 1/2H_2(g)$	0.078	0.679	0.429	0.300
	$C_7H_8^* \longrightarrow C_7H_8(g)$	2.862	2.862	2.784	2.184
demeth.	$[C_7H_8^* \longrightarrow C_6H_5^* + CH_3^*]^‡$	2.341	2.932	2.263	2.253
	$C_7H_8^* \longrightarrow C_6H_5^* + CH_3^*$	1.359	1.996	1.281	1.317
	$C_6H_5^* + CH_3^* + H_2(g) \longrightarrow C_6H_6^* + CH_4^*$	−0.647	−0.284	−2.006	−2.280
	$C_6H_6^* + CH_4^* \longrightarrow C_6H_6(g) + CH_4(g) + *$	2.279	2.279	2.925	2.563
total	$C_7H_8^* + H_2(g) \longrightarrow C_6H_6^* + CH_4^*$			−0.725	−0.963
	$C_7H_{14}^* + \longrightarrow C_7H_8^* + 3\,H_2(g)$			0.078	0.679
	$C_7H_{14}(g) \longrightarrow C_7H_8(g) + 3\,H_2(g)$			2.864	2.864
	$C_7H_{14}(g) \longrightarrow C_6H_6(g) + CH_4(g) + 2\,H_2(g)$			2.279	2.279

[a] Electronic energy relative Pt(111). [b] Electronic energy relative Pt(111) modified with 3/16 ML sulfur.
[c] Reaction energy on pristine Pt(111). [d] Reaction energy on Pt(111) modified with 3/16 ML sulfur.

Table S6 Spin polarization of gas phase molecules and atoms.

Molecule/atom	Spin polarization (yes/no)
C_7H_{14}	no
C_7H_{13}	yes
C_7H_{12}	no
C_7H_{11}	yes
C_7H_{10}	no
C_7H_9	yes
C_7H_8	no
C_6H_6	no
C_6H_5	yes
CH_4	no
CH_3	yes
H_2	no
H	yes
S	yes
O	yes

Adsorption configurations and co-adsorption energies of all reaction intermediates are shown in Table S7. The co-adsorption energy of adsorbates X and Y is defined as:

$$E_{\text{co-ads}} = E_{\text{X,Y/slab}} - E_{\text{slab}} - E_{\text{X}}(\text{g}) - \text{E}_{\text{Y}}(\text{g}) \tag{3}$$

where $E_{\text{X,Y/slab}}$, E_{slab}, $E_{\text{X}}(\text{g})$ and $E_{\text{Y}}(\text{g})$ are the electronic energies of X,Y/Pt(111), Pt(111), gas phase X and gas phase Y, respectively.

Table S7 also includes the difference in (co-)adsorption energies of X and Y between sulfur-modified and pristine Pt(111), given by:

$$\Delta E_{\text{co-ads}} = E_{\text{co-ads}}^{\text{X, Y, S/Pt(111)}} - E_{\text{co-ads}}^{\text{X, Y/Pt(111)}} \tag{4}$$

Here, $E_{\text{co-ads}}^{\text{X, Y, S/Pt(111)}}$ is the co-adsorption energy of X and Y on sulfur-modified Pt(111) and $E_{\text{co-ads}}^{\text{X, Y/Pt(111)}}$ is the co-adsorption energy of X and Y on pristine Pt(111). As illustrated in Fig. S8, sulfur destabilizes dehydrogenation intermediates, with the magnitude of the effect increasing as the degree of chemisorption increases. The degree of chemisorption is here defined by the number of covalent C-Pt bonds. Accordingly, excluding demethylation products, C_7H_{14} is the least chemisorbed intermediate (zero C–Pt bonds), whereas C_7H_8 is the most strongly chemisorbed (three C–Pt bonds). Note, however, that there is no obvious trend between the degree of chemisorption and the (co-)adsorption energies of intermediates, as intermediates with unpaired electrons will always bind strongly to the surface.

Table S7 Adsorption sites and adsorption energies of dehydrogenation intermediates.

Adsorbate	Final adsorption site	[a]$E_{\text{co-ads}}$ (eV)	[b]$E_{\text{co-ads}}$ (eV)	[c]$\Delta E_{\text{co-ads}}$
C_7H_{14}	fcc hollow C1 y	−1.49	−1.49	+0.00
C_7H_{13}, H	fcc hollow C1 y, top	−5.83	−5.73	+0.10
C_7H_{13}	fcc hollow C1 y	−3.20	−3.15	+0.05
C_7H_{12}, H	fcc hollow C1 y, top	−5.09	−4.88	+0.17
C_7H_{12}	fcc hollow C1 y	−2.29	−2.23	+0.06
C_7H_{11}, H	fcc hollow C1 y, top	−9.41	−9.15	+0.26
C_7H_{11}	fcc hollow C1 y	−6.79	−6.60	+0.19
C_7H_{10}, H	fcc hollow C1 xy, top	−6.40	−6.01	+0.39
C_7H_{10}	fcc hollow C1 xy	−3.76	−3.50	+0.26
C_7H_9, H	diagonal bridge C1 xy, fcc	−6.84	−6.05	+0.79
C_7H_9	diagonal bridge C1 xy	−4.04	−3.57	+0.47
C_7H_8, H	diagonal bridge C1 y, top	−5.48	−4.75	+0.73
C_7H_8	diagonal bridge C1 y	−2.78	−2.18	+0.60
C_6H_5, CH_3	diagonal bridge C1 xy, top C-down	−6.35	−5.71	+0.66
C_6H_6, CH_4	diagonal bridge y, top C-down	−2.93	−2.56	+0.37

[a] Pristine Pt(111). [b] Pt(111) modified with 3/16 ML sulfur.
[c] Difference in adsorption energy between pristine and sulfur-modified Pt(111).

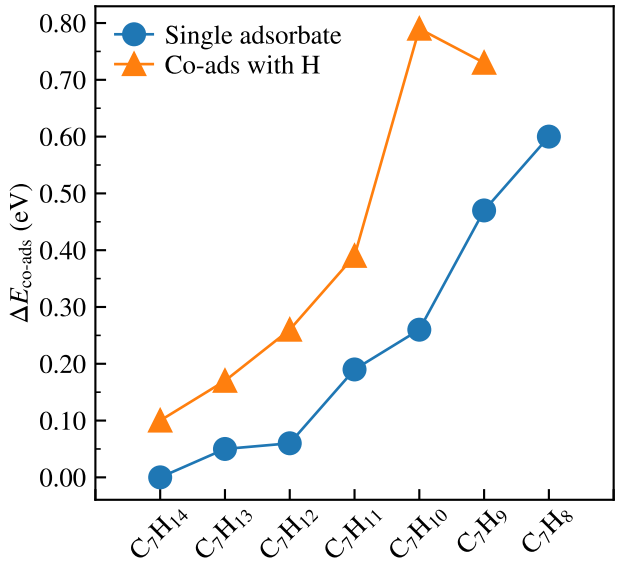

Fig. S8 Difference in (co-)adsorption energy between sulfur-modified and pristine Pt(111).

Sulfur coverage and dehydrogenation kinetics

The optimal sulfur coverage for dehydrogenation of C_7H_{14} was determined by investigating the configurational space of 1-5 sulfur atoms on the surface. For each number of sulfur atoms

n, the search was initiated from the most stable configuration of $n-1$ atoms, resulting in the sulfur configurations shown in Fig. S9. Comparing the adsorption energies of sulfur at the various coverages, it is evident that a sulfur coverage of 4/16 ML, is attainable on Pt(111); at higher coverages, multiple sulfur atoms will be forced to share metal sites, causing a significant increase in adsorption energy. The dehydrogenation reaction was modeled using a coverage of 3/16 ML sulfur atoms, as higher coverages inhibits co-adsorption with C_7H_{14} and C_7H_8 (see Fig. S10). Adsorption energies of sulfur, C_7H_{14} and C_7H_8 at all considered sulfur coverages are summarized in Table S8 .

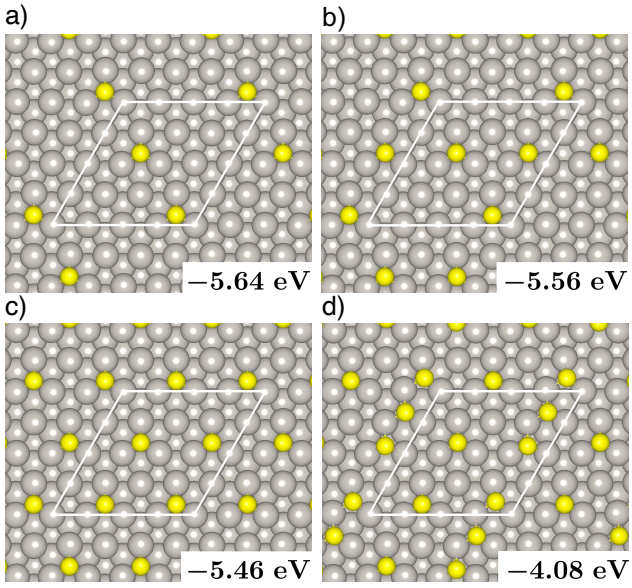

Fig. S9 Adsorption configurations and energies of sulfur at 2/16, 3/16, 4/16 and 5/16 ML coverages on Pt(111). There are more favorable configurations for 5/16; the shown configuration corresponds to adding a sulfur atom to the optimized 4/16 layer.

Table S8 Adsorption energies of C_7H_{14}, C_7H_8 and sulfur at varying sulfur coverages on Pt(111).

Sulfur coverage (ML)	$E_{ads}(C_7H_{14})$ (eV)	$E_{ads}(C_7H_8)$ (eV)	$E_{ads}(S)$ (eV)
0	−1.49	−2.78	–
1/16	−1.49	−2.58	−5.73
2/16	−1.47	−2.40	−5.64
3/16	−1.46	−2.26	−5.56
4/16	−0.92	−0.83	−5.46
5/16	–	–	−4.08

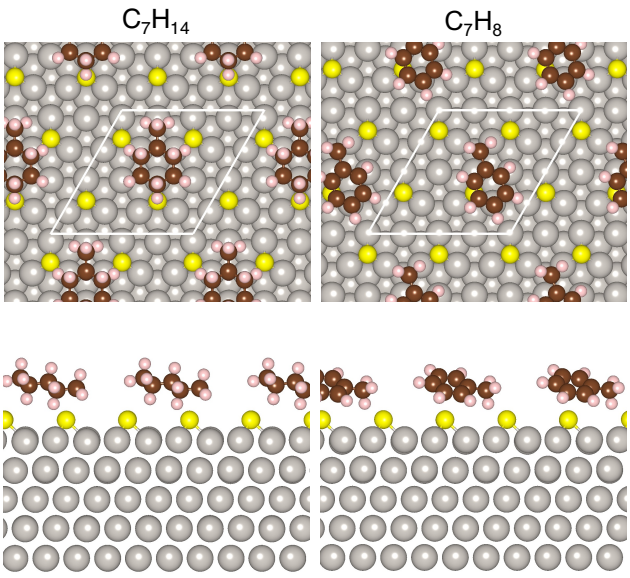

Fig. S10 Adsorption configurations of C_7H_{14} (left) and C_7H_8 (right) on Pt(111) modified with 4/16 ML sulfur) from the top (upper) and the side (lower).

Transition states

Transition states for $C_7H_8{}^* \longrightarrow C_6H_5{}^* + CH^*$ over Pt(553) were obtained using the nudged elastic band (NEB) and climbing image schemes.[5] As described in the main text, NEB trajectories were created in two sets, where the final configuration for the second set was selected after partial convergence of the first set. The search for the transition state along trajectory C (rotation of C_7H_8 toward the upper terrace and CH_3 occupying a top site at the upper terrace) is schematically illustrated in Fig. S11. Here, C_7H_8 was first rotated from its most stable adsorption configuration into the initial configuration of the NEB trajectory. This rotation was also adopted for C_6H_5 in the final configuration along the trajectory. Thereafter, a set of 7 intermediate images was created and relaxed. A new final configuration was then selected from the intermediate images and a second set of five intermediate images was generated. This set was relaxed using the climbing image approach and a transition state was identified as the image corresponding to the maximum energy along the minimum energy path. The activation barrier to reach the transition state was calculated as the sum of

the energy penalty to rotate C_7H_8 into the initial configuration of the trajectory (0.012 eV), and the difference in energy between this configuration and the transition state (2.19 eV), amounting to 2.20 eV. The thermodynamic reaction energy was calculated as the difference in electronic energy between the most stable configuration of C_7H_8 and the most stable configuration of C_6H_5 + CH_3. Transition states A and B were obtained in a similar fashion. To reach transition state A, C_7H_8 was was first rotated into the initial configuration of the NEB trajectory at an energy cost of 0.21 eV, whereas the trajectory for transition state B was initiated from the most stable configuration of C_7H_8.

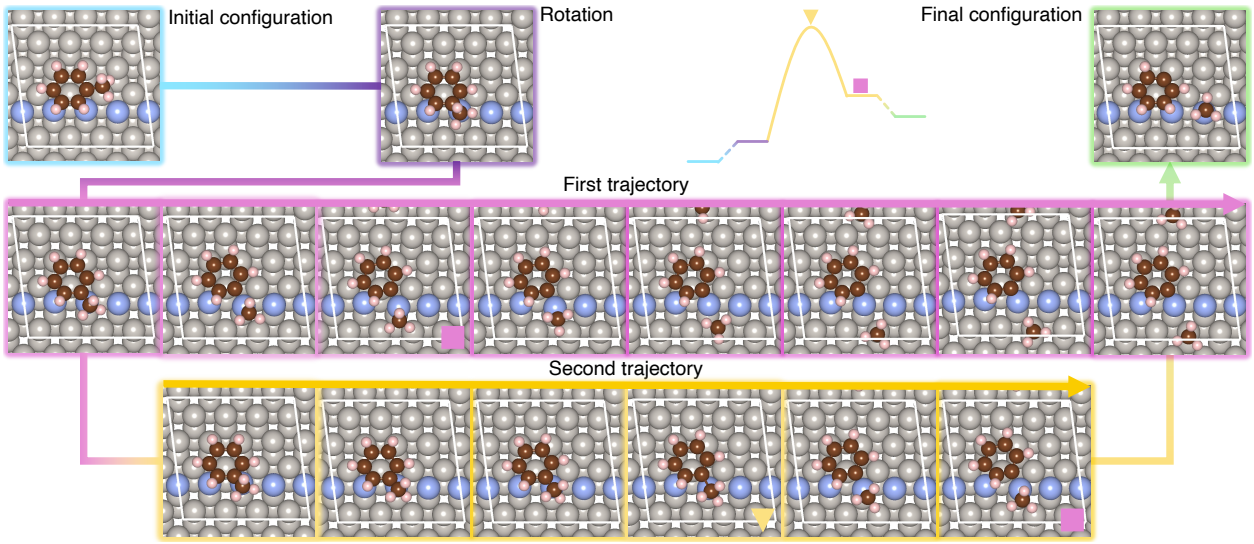

Fig. S11 Schematic illustration of NEB trajectory C. From the initial configuration (blue), C_7H_8 was rotated towards the upper terrace (purple) and a NEB path with seven intermediate images was created (pink). From this trajectory, a new final state (pink square) was selected, relaxed and used as the end point for a new NEB trajectory (yellow). The most stable configuration of the final fragments is shown in green, and the transition state is marked by a yellow triangle.

Microkinetic modeling

Reaction kinetics are evaluated within the mean-field approximation. The overall reaction is separated into reaction steps and the rate of each step is assumed to be proportional to

the surface coverage of the reacting species j:

$$\frac{d\theta_j}{dt} = \sum_a c_{ju} r_u \left(\vec{\theta}\right) \tag{5}$$

where θ_j is the surface coverage, c_{ja} is the number of j molecules in reaction u and $r_u\left(\vec{\theta}\right)$ is the coverage-dependent reaction rate for reaction u. Thus, the kinetic evolution of the reaction is described a set of coupled ordinary differential equations (ODE's), which are numerically integrated to yield steady state surface coverages at given reaction conditions. The integration is performed using the LSODA Scipy ODE solver for initial value problems, which includes automatic switching between Adams and backward differentiation.[6,7]

Adsorption steps are treated as unactivated processes, where the rate constant associated with adsorption of species j (k_j^{ads}) is calculated from kinetic gas theory:[8]

$$k_j^{\mathrm{ads}} = \frac{p_j A_{\mathrm{site}}}{\sqrt{2\pi m_j k_{\mathrm{B}} T}} \tag{6}$$

Here, p_j is the partial gas-phase pressure, m_j is the molecular mass, k_{B} is Boltzmann's constant, T is the temperature and A_{site} is the surface area of an adsorption site (set to $10\,\mathrm{\AA}^2$). Thermodynamic consistency is guaranteed by calculating the desorption rate constant (k_j^{des}) from the forward rate constant (k_j^{ads}) and the equilibrium constant (K_j):

$$k_j^{\mathrm{des}} = \frac{k_j^{\mathrm{ads}}}{K_j} = k_j^{\mathrm{ads}} \exp\left(\frac{\Delta G_j\left(T,p\right)}{k_{\mathrm{B}} T}\right) \tag{7}$$

where ΔG_j is the change in Gibbs free energy upon reaction. The entropy contribution to the gas-phase Gibbs free energy is calculated from thermodynamic tables for H_2,[9] and from the partition functions for the carbon-based molecules.[10–12] The entropy for the adsorbed species is computed using the vibrational partition functions within the harmonic approximation.[8]

The surface reactions are treated within harmonic transition state theory and rate con-

stants are calculated as:[13]

$$k_{\mathrm{TST}} = \frac{k_{\mathrm{B}}T}{h}\frac{q_0^{\ddagger}}{q}\exp\left(-\frac{\Delta E_{\mathrm{a}}}{k_{\mathrm{B}}T}\right) \tag{8}$$

Here, h is Planck's constant, $q_0^{\ddagger}$ is the transition state partition function referenced to its own electronic ground state. q is the partition function of the initial state, and ΔE_{a} is the activation barrier of the reaction.

The reaction order (n_j) is calculated to obtain the dependence of the reaction kinetics on the concentration of reacting species j:

$$n_j = p_j\frac{\partial\left[\ln\left(r_{\mathrm{x}}\right)\right]}{\partial p} \tag{9}$$

where p_j is the partial pressure and r_{x} is the net rate of the reaction. The apparent activation energy (E_{app}) is calculated as:[8]

$$E_{\mathrm{app}} = k_{\mathrm{B}}T^2\frac{\partial\ln(r_{\mathrm{x}})}{\partial T} \tag{10}$$

The sensitivity of the net reaction rate to each elementary step i is evaluated by calculating the degree of rate control (DRC, χ_i):[14]

$$\chi_i = \frac{k_i}{r_{\mathrm{x}}}\left(\frac{\partial r_{\mathrm{x}}}{\partial k_i}\right)_{K_i} \tag{11}$$

where k_i denotes the rate constant, r_{x} is the net reaction rate, and K_i is the equilibrium constant. The derivative is evaluated with respect to the rate constant while keeping K_i constant. This is done numerically by differentiating the rate with respect to the rate constant, using a change of 10% in the rate constant. A positive or negative value of χ_i shows that the elementary step enhances or suppresses the net rate, respectively. The sum of χ_i over all elementary steps add up to one. A value of one for any single step signifies that the step is rate-controlling[14]

Kinetic simulations

Mean-field microkinetic modeling was used to evaluate the effect of sulfur on the rate of dehydrogenation of C_7H_{14} to C_7H_8 on Pt(111). The kinetic model used here is a reduced version of the one reported in Ref. 15. Here, the dehydrogenation of C_7H_{14} and the hydrodemethylation of C_7H_8 are represented as lumped reactions, (R1) and (R2):

$$C_7H_{14}^* + 6* \rightleftharpoons C_7H_8^* + 6\,H^* \quad \text{(R1)}$$

$$C_7H_8^* + 2\,H^* \rightleftharpoons C_6H_6 + CH_4(g) \quad \text{(R2)}$$

Thus, the reaction intermediates are C_7H_{14}, C_7H_8, benzene (C_6H_6), and hydrogen (H). This simplification is schematically illustrated in Fig. S12.

Reaction and adsorption energies of the included species were obtained from the DFT-calculated values in Table S5 and Table S7. The rate constants k_{TST} (Eq. (8)) of the simplified reactions (R1) and (R2) were calculated using pre-exponential factors approxi-

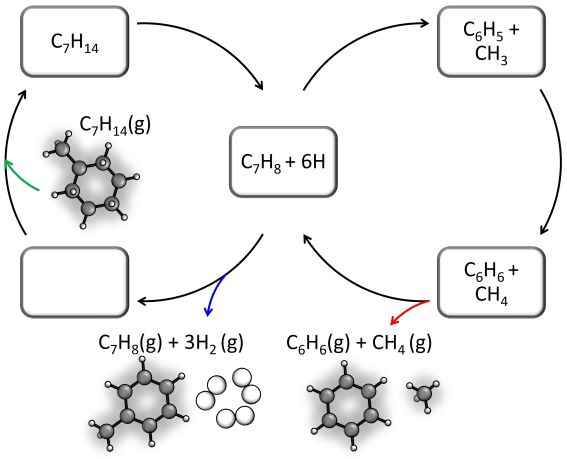

Fig. S12 Schematic of the simplified dehydrogenation of C_7H_{14} and hydrodemethylation of C_7H_8 over Pt(111). Adsorption of C_7H_{14} is indicated by a green arrow, dehydrogenation products are indicated by a blue arrow, and hydrodemethylation products with a red arrow. The empty box represents the pristine surface.

mated from the partition functions of the dehydrogenation of C_7H_{14} to C_7H_{13} + H and the demethylation of C_7H_8, respectively, as calculated in Ref. 15. The forward activation barrier for reaction (R1) was approximated as the highest activation barrier among the surface-bound dehydrogenation steps, as reported in Ref. 15. The corresponding backward barrier was approximated as the sum of the forward barrier and the energy gain (0.68 eV) of co-adsorbing 6H on the surface. For reaction (R2), the explicit barriers reported Ref 15 were used. All elementary steps, activation energies, and pre-exponential factors (calculated at 673 K) from which the microkinetic model was constructed are summarized in Table S9.

In the microkinetic model (and in Table S9), Pt(111) modified with 0.19 ML sulfur is used as a reference system. A change in the sulfur coverage is represented by a change in the energetics. As discussed in the main text, the presence of $0 - 0.19$ ML sulfur on the catalyst surface does not change the adsorption energy of C_7H_{14}, whereas the adsorption energy of C_7H_8 decreases linearly. Moreover, the rate of hydrodemethylation of C_7H_8 to C_6H_6 and CH_4 depends directly on the coverage of C_7H_8.[15] Therefore, the microkinetic model assumes that sulfur coverages between 0 and 0.19 ML only affects the adsorption energy of C_7H_8. Modifying the adsorption energy of only one reacting species directly alters the relative stability of the gas-phase and the adsorbed molecule (C_7H_8). To maintain thermodynamic consistency, all elementary steps (and their activation barriers) directly involving toluene are adjusted to

Table S9 Elementary steps in the reaction network and calculated kinetic parameters: forward ($\Delta E_{a,f}$) and backward ($\Delta E_{a,b}$) activation barriers, and pre-exponential factors[a] on sulfur-modified Pt(111). Activation barriers are reported for sulfur coverages of [0.00 ML], 0.19 ML and (0.25 ML).

No.	Reaction	$\Delta E_{a,f}$	$\Delta E_{a,b}$ (eV)	A_f	A_b
R1	$C_7H_{14}^* + 6* \rightleftharpoons C_7H_8^* + 6\,H^*$	1.20	[2.40] 1.88 (1.68)	2.67×10^{14}	1.42×10^{13}
R2	$C_7H_8^* + 2\,H^* \rightleftharpoons C_6H_6^* + CH_4(g)$	2.21	1.65	1.02×10^{14}	1.31×10^{13}
R3	$C_7H_{14}(g) + * \rightleftharpoons C_7H_{14}^*$	0.00	[1.46] 1.46 (1.26)	4.31×10^{2}	1.94×10^{11}
R4	$C_7H_8^* \rightleftharpoons C_7H_8(g) + *$	[2.78] 2.18 (2.06)	0.00	1.36×10^{7}	4.45×10^{2}
R5	$C_6H_6^* \longrightarrow C_6H_6(g) + *$	2.32	—	1.36×10^{13}	—
R6	$H_2(g) + 2* \rightleftharpoons 2\,H^*$	0.00	1.00	3.02×10^{3}	1.26×10^{7}

[a] Pre-exponential factors are calculated at 673 K and are denoted A_f and A_b for forward and backward reactions, respectively. The pre-exponential factors of surface reactions are reported in (s^{-1}), whereas adsorption steps are reported in ($Pa^{-1}s^{-1}$).

reflect the modified adsorption energy. The model also assumes that sulfur does not compete for sites with the reaction intermediates. As the carbon-based molecules occupy more than one metal site upon adsorption, the maximum total coverage of carbon-based molecules was fixed to 0.11 ML. This value is consistent with the previous DFT-calculations[15] and experimentally observed saturation coverages.[16,17]

Effect of sulfur coverage on kinetics and rates

The turnover frequency (TOF) as a function of the sulfur coverage is reported in the main text. In addition, we have evaluated the details of the reaction kinetics of C_7H_{14} dehydrogenation at sulfur coverages of i) 0.00 ML, ii) 0.19 ML and iii) 0.25 ML on Pt(111). The calculations were performed in the temperature range $573-923$ K, using $p[C_7H_{14}] = 1.00$ bar and considering 5% conversion to $C_7H_8 + H_2$ and 1% conversion to $C_6H_6 + CH_4$.

TOFs, coverages, DRCs, reaction orders and apparent activation energies are reported in Fig. S13-S15. The TOF increases with the sulfur coverage between 0.00 ML and 0.19 ML, but decreases dramatically at higher coverages. The temperature corresponding to the maximum TOF decreases from 817 K at 0.00 ML to 769 K at 0.19 ML. This enhancement in activity and shift to lower temperature are associated with reduced C_7H_8 coverage in the presence of sulfur. Note that on pristine Pt(111), the C_7H_8 coverage approaches saturation prior to light-off.

The kinetic behavior is similar for the three cases. The surface is covered mainly by hydrogen and C_7H_8, and light-off coincides with a decline in C_7H_8 coverage. DRC analysis shows that the dehydrogenation steps control the reaction in the entire temperature range. The reaction order in C_7H_{14} is close to unity, whereas the reaction order in hydrogen is close to zero. The apparent activation energy (E_{app}) decreases with temperature; before light-off, E_{app} for the dehydrogenation reaction is about 3.5 eV, consistent with the sum of the dehydrogenation barrier and the C_7H_8 desorption energy (Table S9). In all three cases, the rate of the demethylation reaction is several orders of magnitude lower than the

rate of the dehydrogenation reaction. Sulfur coverages up to 0.19 ML further suppress the demethylation reaction.

These results highlight that the main effect of sulfur is destabilization of chemisorbed species through electronic modification of the Pt surface. Sulfur coverages of up to 0.19 ML promote desorption of C_7H_8, which prevents demethylation and also allows for a higher TOF by freeing up reaction sites.

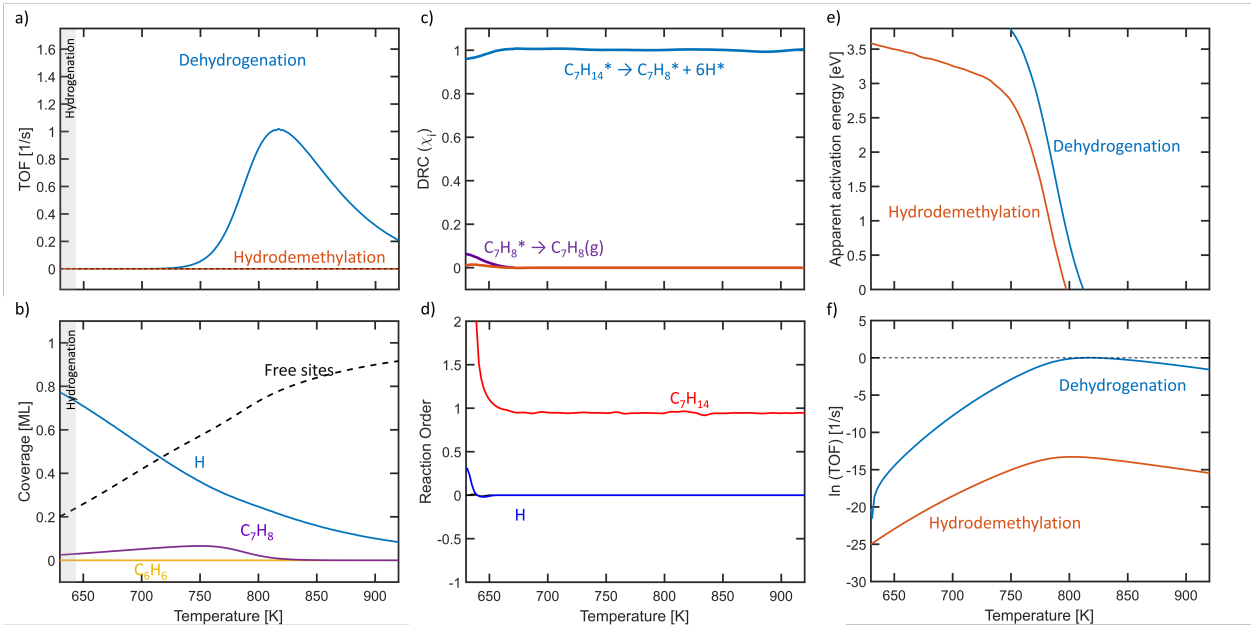

Fig. S13 Temperature-dependent kinetic analysis of C_7H_{14} dehydrogenation on pristine Pt(111): a) surface coverage, b) TOF, (c) DRC, d) reaction orders, e) apparent activation energy, f) logarithm of the TOF. The simulations were performed using $T = 573 - 923$ K, p[C_7H_{14}] = 1.00 bar, 5% conversion to $C_7H_8 + H_2$, and 1% conversion to $C_6H_6 + CH_4$.

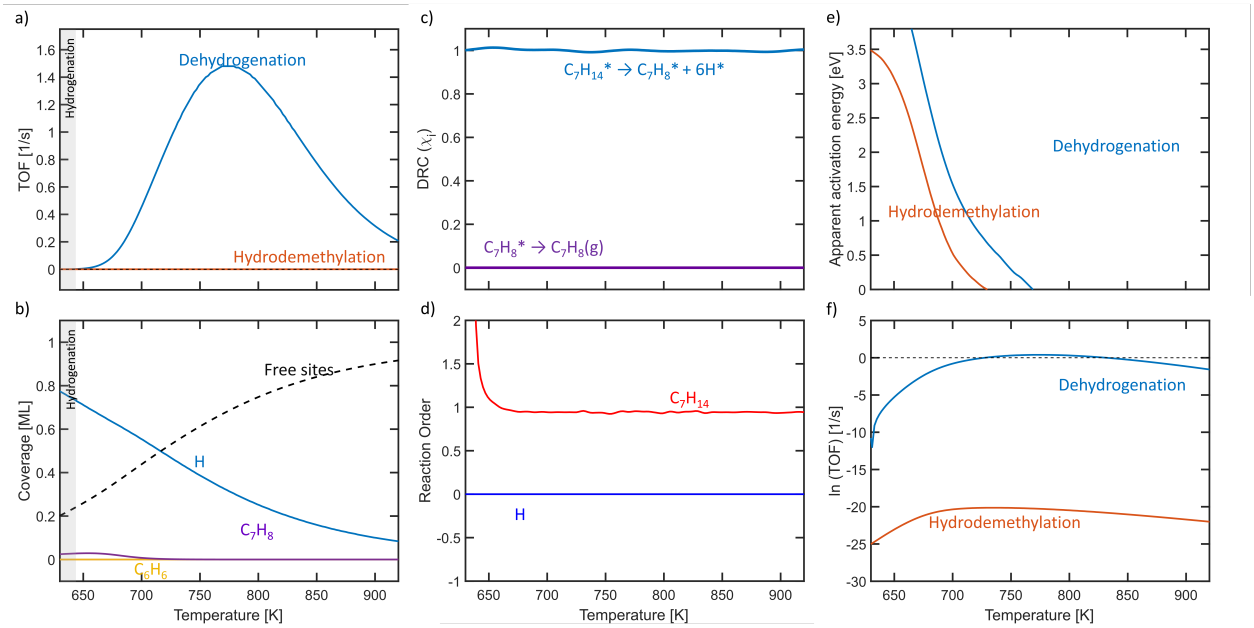

Fig. S14 Temperature-dependent kinetic analysis of C_7H_{14} dehydrogenation on Pt(111) modified with 0.19 ML sulfur: a) surface coverage, b) TOF, (c) DRC, d) reaction orders, e) apparent activation energy, f) logarithm of the TOF. The simulations were performed using $T = 573 - 923$ K, p[C_7H_{14}] = 1.00 bar, 5% conversion to C_7H_8 + H_2, and 1% conversion to C_6H_6 + CH_4.

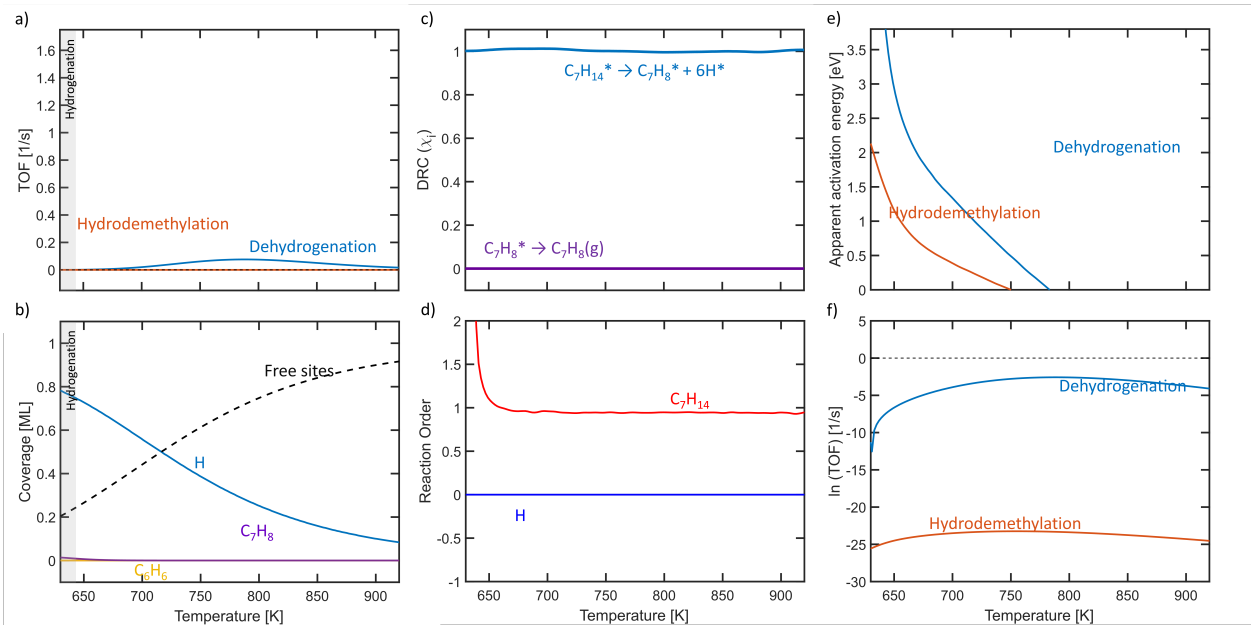

Fig. S15 Temperature-dependent kinetic analysis of C_7H_{14} dehydrogenation on Pt(111) modified with 0.25 ML sulfur: a) surface coverage, b) TOF, (c) DRC, d) reaction orders, e) apparent activation energy, f) logarithm of the TOF. The simulations were performed using $T = 573 - 923$ K, p[C_7H_{14}] = 1.00 bar, 5% conversion to C_7H_8 + H_2, and 1% conversion to C_6H_6 + CH_4.

References

(1) Mavrikakis, M.; Hammer, B.; Nørskov, J. K. Effect of Strain on the Reactivity of Metal Surfaces. *Phys. Rev. Lett.* **1998**, *81*, 2819–2822.

(2) Hjorth Larsen, A.; others The Atomic Simulation Environment – A Python library for working with atoms. *J. Phys.: Condens. Matter* **2017**, *29*, 273002.

(3) Auer, F.; Blaumeiser, D.; Bauer, T.; Bösmann, A.; Szesni, N.; Libuda, J.; Wasserscheid, P. Boosting the Activity of Hydrogen Release from Liquid Organic Hydrogen Carrier Systems by Sulfur-Additives to Pt on Alumina Catalysts. *Catal. Sci. Technol.* **2019**, *9*, 3537–3547.

(4) Saeys, M.; Reyniers, M.-F.; Marin, G. B.; Neurock, M. Density Functional Study of Benzene Adsorption on Pt(111). *J. Phys. Chem. B* **2002**, *106*, 7489–7498.

(5) Henkelman, G.; Uberuaga, B. P.; Jónsson, H. A Climbing Image nudged Elastic Band Method for Finding Saddle Points and Minimum Energy Paths. *J. Chem. Phys.* **2000**, *113*, 9901–9904.

(6) Hindmarsh, A. C. In *Scientific Computing*; Stepleman, R. S., others, Eds.; North-Holland: Amsterdam, 1983; pp 55–64.

(7) Petzold, L. Automatic Selection of Methods for Solving Stiff and Nonstiff Systems of Ordinary Differential Equations. *SIAM J. Sci. Stat. Comput.* **1983**, *4*, 136–148.

(8) Chorkendorff, I.; Niemantsverdriet, J. W. *Concepts of Modern Catalysis and Kinetics*, 3rd ed.; Wiley-VCH: Weinheim, 2017.

(9) Linstrom, P. J.; Mallard, W. G. NIST Chemistry WebBook; NIST Standard reference database number 69; National Institute of Standards and Technology: Gaithersburg, MD. `http://webbook.nist.gov`, 2005; Accessed: 11 Dec 2020.

(10) Delley, B. An All-Electron Numerical Method for Solving the Local Density Functional for Polyatomic Molecules. *J. Chem. Phys.* **1990**, *92*, 508–517.

(11) Delley, B. From Molecules to Solids with the DMol^3 Approach. *J. Chem. Phys.* **2000**, *113*, 7756–7764.

(12) BIOVIA, D. S. Materials Studio, Version 2020. Dassault Systèmes: San Diego, CA, 2020; DMol^3 module used for calculations.

(13) Eyring, H. The Activated Complex in Chemical Reactions. *J. Chem. Phys.* **1935**, *3*, 107–115.

(14) Campbell, C. T. The Degree of Rate Control: A Powerful Tool for Catalysis Research. *ACS Catal.* **2017**, *7*, 2770–2779.

(15) Posada-Borbón, A.; Möslinger, T.; Grönbeck, H. Reaction kinetics of liquid organic hydrogen carriers from first-principles: The methylcyclohexane/toluene pair on Pt(111). *ChemRxiv* **2026**, preprint.

(16) Jiang, L.; Koel, B. E. Hydrocarbon Trapping and Condensation on Platinum (111). *J. Phys. Chem.* **1992**, *96*, 8694–8697.

(17) Gottfried, J. M.; Vestergaard, E. K.; Bera, P.; Campbell, C. T. Heat of Adsorption of Naphthalene on Pt(111) Measured by Adsorption Calorimetry. *J. Phys. Chem. B* **2006**, *110*, 17539–17545.